AIAA Aviation Forum and ASCEND co-located Conference Proceedings
21 - 25 July 2025, Las Vegas, Nevada
AIAA AVIATION FORUM AND ASCEND 2025

10.2514/6.2025-3080

Variation in Sonic Boom Metrics due to Atmospheric Turbulence during CarpetDIEM III

Kaylee Nyborg[1] and Kent L. Gee[2]
Brigham Young University, Provo, Utah, 84602, USA

Alexandra Loubeau[3]
NASA Langley Research Center, Hampton, VA, 23681, USA

The Carpet Determination In Entirety Measurement (CarpetDIEM) III campaign provided insights into the variability of sonic boom metrics due to atmospheric turbulence. ARray Instrumentation for Sonic Thump Observations in TurbuLEnce (ARISTOTLE) Jr., a 2D array consisting of 23 microphones, recorded 17 sonic booms during the measurement campaign. On average, the Perceived Level (PL) across the array had a range of 7.3 dB and a standard deviation of 1.7 dB. While high wind speeds coincided with the largest PL range, significant variability also occurred during lower wind conditions, suggesting ambient noise and atmospheric turbulence play a role in the variability of metrics. The data further indicated directional dependency in metric variability, affirming the necessity of a 2D measurement approach. Building on these results, a full-scale ARISTOTLE array, consisting of 61 microphones over an area of 1,000 ft x 1,000 ft (305 m x 305 m) is under development and will be used in a future low-boom measurement campaign. Ultimately, ARISTOTLE will support the characterization of signatures generated by the X-59 aircraft, enabling improved understanding of turbulence effects on sonic boom metrics.

I. Nomenclature

u_*	=	friction velocity
w_*	=	mixed-layer velocity scale
σ_{vector}	=	velocity fluctuations due to turbulence
1D	=	one-dimensional
2D	=	two-dimensional
AFRC	=	Armstrong Flight Research Center
ARISTOTLE	=	ARray Instrumentation for Sonic Thump Observations in TurbuLEnce
ARISTOTLE Jr.	=	Subset of ARISTOTLE
ASEL	=	A-weighted Sound Exposure Level
BLM	=	Bureau of Land Management
BSEL	=	B-weighted Sound Exposure Level
CarpetDIEM	=	Carpet Determination In Entirety Measurement
DSEL	=	D-weighted Sound Exposure Level
ESEL	=	E-weighted Sound Exposure Level

[1] Ph.D. Candidate, Department of Physics and Astronomy, Student Member
[2] Professor and Chair, Department of Physics and Astronomy, Associate Fellow
[3] Research Aerospace Engineer, Applied Acoustics Branch

ISBAP	=	Indoor Sonic Boom Annoyance Predictor
NASA	=	National Aeronautics and Space Administration
PL	=	Perceived Level
SNR	=	Signal-to-Noise Ratio
SonicBAT	=	Sonic Booms in Atmospheric Turbulence

II. Introduction

The National Aeronautics and Space Administration (NASA) Quesst mission marks a notable advancement toward enabling supersonic commercial overland flight. The primary objectives of the Quesst mission are to demonstrate quieter sonic booms with the experimental X-59 aircraft and to survey the community response. The quieter sonic booms, referred to as shaped booms or sonic thumps, should have lower amplitudes and longer rise times (i.e., less high-frequency energy) than N-waves. The low-noise signature data will be shared with regulators to inform their potential decisions on new noise standards and lift the present overland commercial supersonic flight ban [1, 2]. As sonic boom noise is the prime barrier to overland supersonic flight [1], accurately measuring metrics of the low-noise signatures with the associated uncertainty is important to inform possible regulation changes.

Atmospheric turbulence affects the loudness of sonic booms heard at the ground [3]. Turbulence, caused by random fluctuations in temperature and wind velocity, can cause spiking, rounding, or other changes to the waveform shape that increase or decrease the overpressure and rise time [3-6]. Because turbulence causes random focusing and defocusing of acoustic energy, the effects are modeled statistically. Although it is difficult to predict the effect of atmospheric turbulence on a single boom, the mean effect is to increase the rise time of the boom [3,7]. This causes a decrease in the level of metrics correlated with human perception [8-11] due to the impact on high-frequency energy and rise time.

In addition to laboratory-scale measurements [12-14], various measurements have been made to study the effect of atmospheric turbulence on N-waves from aircraft. One extensive analysis of 1960s NASA test data was that of Ref. [5], which developed a physical model to investigate the interaction of sonic booms with turbulence. They performed scattering calculations to demonstrate that eddies of various scales were effective in producing long rise times and many non-N boom waveform shapes. The NASA test campaign Sonic Booms in Atmospheric Turbulence (SonicBAT) produced a substantial database of sonic boom data and atmospheric turbulence parameters [10, 15]. As part of a larger campaign including 125 flights and over 4,000 boom recordings, SonicBAT studied the effects of atmospheric turbulence on N-waves. The primary ground-based microphone array was linear and nominally consisted of sixteen microphones with 100 ft (30.5 m) spacing, and the secondary and tertiary arrays were cross arrays composed of eight microphones with 100 ft spacing [10]. On a smaller scale, a microphone array intended to examine turbulence effects was deployed during the first phase of Carpet Determination In Entirety Measurement (CarpetDIEM I) [16]. The primary array was a large, lateral array perpendicular to the flight track with up to 17 microphones across up to 15 nautical miles. Additionally, a subset of measurements was made at a higher spatial resolution. This subset array was also perpendicular to the flight track and consisted of seven microphones with either 50 ft (15.2 m) or 100 ft (30.5 m) spacing. The observed variability in Perceived Level (PL) across microphones with smaller spacing was more than 11 dB.

Tests with the X-59 will soon present opportunities to measure the effects of atmospheric turbulence on shaped booms. ARray Instrumentation for Sonic Thump Observations in TurbuLEnce (ARISTOTLE) is one measurement system that will be used to characterize variation due to atmospheric turbulence. The fundamental ARISTOTLE design is derived from recommendations and observations in literature. Different array designs were explored in a numerical study on shaped booms to measure the variability of metrics due to atmospheric turbulence. Ref. [8] used PL spatial maps in a Monte Carlo experiment to investigate variations of three deterministic array types: linear, cross, and grid. The number of microphones and the microphone separation distance were varied for each type of array. The results suggest that the spatial field must be sampled with sufficient density over a large enough aperture to accurately represent the boom level and its uncertainty. For the cases studied, the two-dimensional (2D) cross array had a more precise PL standard deviation and a more accurate mean than the one-dimensional (1D) linear and 2D grid arrays. The spacing between microphones was informed by the results of a flight test conducted with an F-104 in steady flight [3]. The recorded pressure signatures were essentially the same for microphones within 25 ft (7.6 m) of each other but were different from each other for microphones spaced 50 ft (15.2 m) apart. Based on these studies, the proposed design for ARISTOTLE is a cross array with microphone spacing ranging from 25 ft (7.6 m) to 50 ft (15.2 m). The design is described in more detail at the end of this paper. ARISTOTLE will be a 2D array with fine spatial resolution and a large span to measure the variation due to atmospheric turbulence.

An opportunity to test the ARISTOTLE concept came in January 2024, during the third phase of the CarpetDIEM campaign (CarpetDIEM III) [17]. Although the primary purposes of this flight test were for NASA to test a new generation of ground recording systems and the logistics of deploying the systems, data were obtained with a subset of ARISTOTLE, dubbed ARISTOTLE Jr. The 2D variability in metrics was measured, and the results can be used to finalize microphone spacing and array size needed for the full array. The test included 17 supersonic overflights with two different maneuvers and three different headings. Although aggregating results is challenging with this limited dataset because uniform flight and meteorological conditions were not present, the challenge of varying conditions is likely to occur in community testing for the X-59. Future test campaigns will include more flights and produce larger datasets but will likely still have varying atmospheric conditions. Lessons learned may be applied to the full-scale array for further preparatory testing and the X-59 measurements.

The purpose of this paper is twofold. The first objective is to quantify the variability of metrics at CarpetDIEM III and relate the variability to physical phenomena such as weather conditions and heading. The second purpose is to use the results with the limited 2D array to guide the final design of ARISTOTLE. An overview of the CarpetDIEM III measurement campaign is given in Section III. The flight trajectories, weather conditions, and microphone array are discussed. The analysis procedure is described in Section IV, and results, including the final ARISTOTLE design, are discussed in Section V. Lastly, conclusions are discussed in Section VI.

III. Measurement Campaign Overview

A. Flights

The CarpetDIEM III test occurred in January 2024 in the Mojave Desert near NASA Armstrong Flight Research Center (AFRC). An F-15 was flown at Mach 1.2 to Mach 1.4 at an altitude of 40,000 ft (12,200 m) to 50,000 ft (15,200 m). Measurements from CarpetDIEM III will be compared with results from the earlier CarpetDIEM I, which involved an F/A-18A at Mach 1.4 at an altitude of 30,000 ft (9,140 m). During CarpetDIEM III, ARISTOTLE Jr. was deployed for five flights, and each flight had three to four passes. Each of the five flights had one of three nominal headings: northbound, eastbound, or westbound. Portions of the transonic and supersonic trajectories of the first pass from each flight are shown in Figure 1 along with NASA stations used for CarpetDIEM III (blue circles) and a red circle representing ARISTOTLE Jr. All passes for a given flight had a similar heading. There were also two maneuvers: supersonic cruise and climbing acceleration. Flights 1 and 5 had supersonic cruise maneuvers and Flights 2, 3, and 4 had climbing acceleration maneuvers.

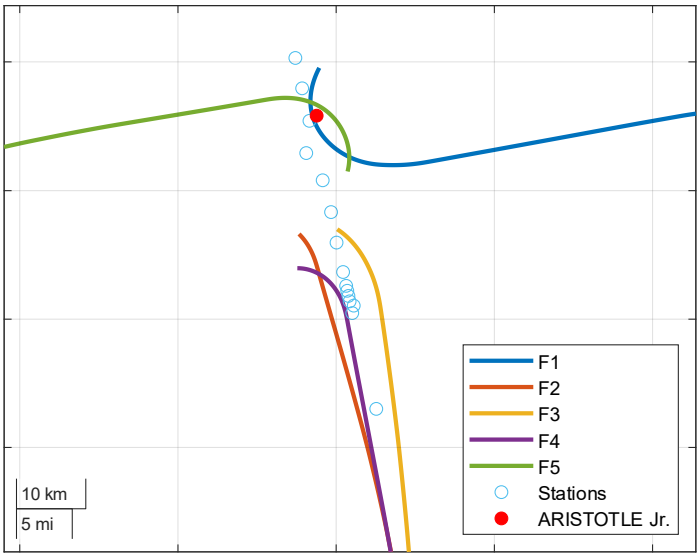

Figure 1. Groundtrack flight trajectories for five F-15 flights, labeled F1 to F5. One flight was eastbound (F5), one westbound (F1), and three northbound (F2, F3, and F4). ARISTOTLE Jr. is located at the northern part of the NASA array.

B. Weather Conditions

Surface weather measurements were made for each flight and pass, and the data are included in Table 1. A Kestrel™ 4600 Heat Stress Tracker was used to measure the surface weather near the center of ARISTOTLE Jr. The temperature varied from 8.9 to 20.2ºC, and the coolest temperatures occurred during the morning flight. The wind speed was the most variable of the surface weather data. Flights 2 and 4 had stronger winds, whereas the other flights had milder winds.

Table 1. Surface weather conditions at ARISTOTLE Jr.

Flight/Pass	Temperature (ºC)	Pressure (hPa)	Wind Speed (m/s)	Wind Direction (deg)
F1 P1	12.5	925.7	0.6	315
F1 P2	12.8	925.7	0.6	304
F1 P3	12.3	923.9	2.0	237
F2 P1	9.0	920.0	5.1	257
F2 P2	8.9	919.8	6.6	250
F2 P3	9.1	920.0	6.7	248
F3 P1	18.7	923.6	0.8	195
F3 P2	16.8	923.7	1.5	172
F3 P3	20.2	923.4	0.4	223
F3 P4	17.4	923.2	1.4	217
F4 P1	18.1	918.3	7.3	229
F4 P2	18.3	918.2	5.3	241
F4 P3	17.9	918.0	6.8	232
F4 P4	18.1	918.0	5.7	237
F5 P1	16.3	925.1	2.0	105
F5 P2	16.0	925.0	1.3	152
F5 P3	16.2	924.8	1.4	105

A weather balloon was launched prior to Flights 1, 2, 3, and 5 approximately 3.5 mi (5.6 km) away from ARISTOTLE Jr., and the data are shown in Figure 2. Flight 4 was an afternoon flight with high winds, which prevented a successful launch of the weather balloon [17]. Trends are similar for temperature and wind speed. Weather balloon data show that wind speeds were lowest for Flight 5. Wind speeds increased for Flights 3, 1, and then 2, which had the highest measured wind speeds. Flight 4 likely had higher wind speeds at altitude given the highest measured wind speeds at the ground.

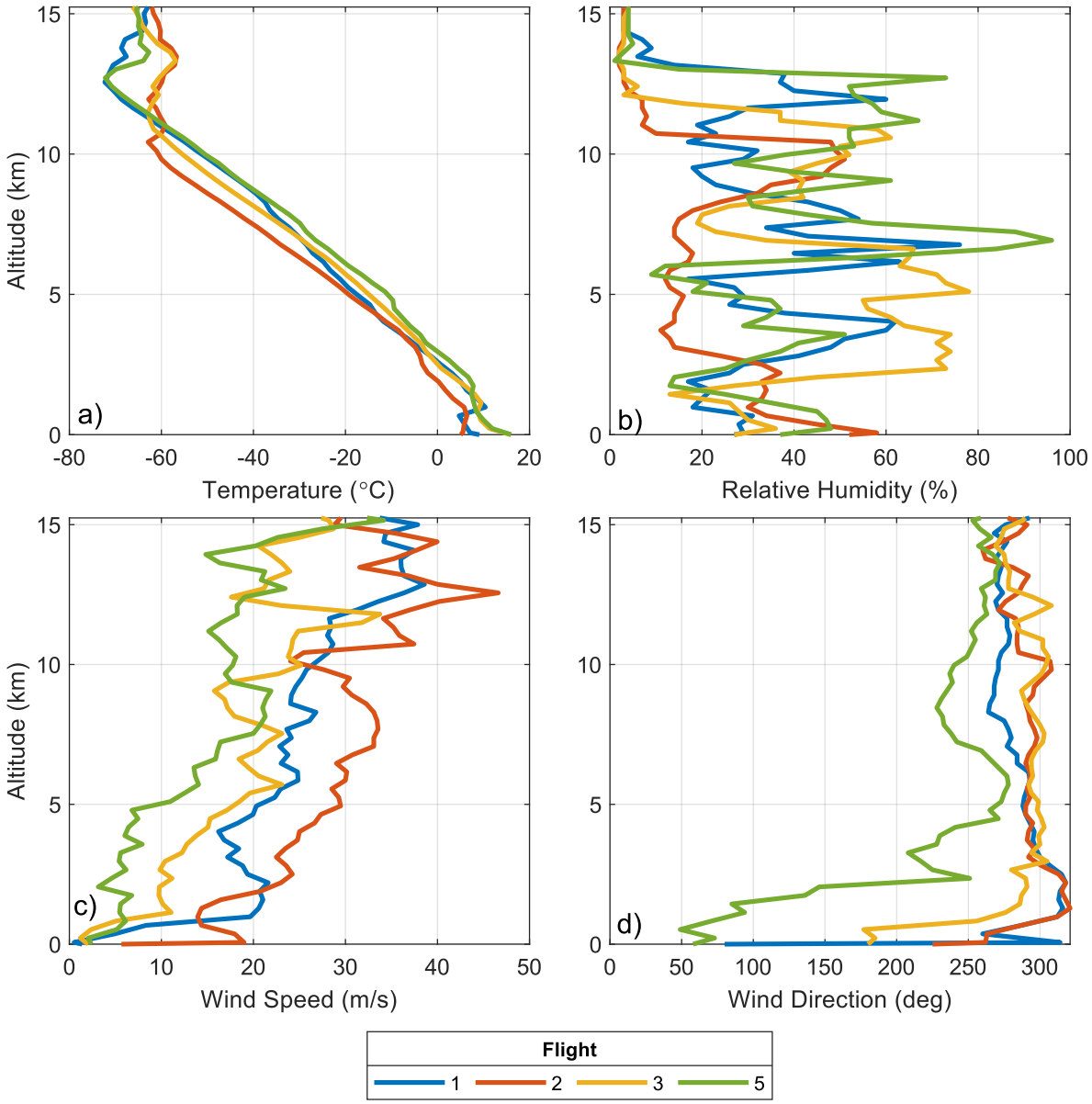

Figure 2. Weather balloon data for Flights 1, 2, 3, and 5.

Turbulence measurements at a height of 30 ft (9.1 m) were also made for the final three flights with a sonic anemometer. Turbulence parameters are included in Table 2. The atmospheric boundary layer (ABL) height was estimated using Climate Forecast System Version 2 (CFSv2) model data [18], which was recently studied in Ref. [19]. CFSv2 ABL heights will be validated against measured ABL heights in future work; however, since ABL measurements were not made for this test, the analysis will rely on modeled data. The friction velocity, u_*, surface layer temperature scale, T_*, mixed-layer velocity scale, w_*, and velocity fluctuations due to turbulence, σ_{vector}, were calculated from the sonic anemometer data. The σ_{vector} values for Flight 4 are higher than those for other flights.

Table 2. Turbulence parameters calculated from sonic anemometer data. The ABL height was obtained from CFSv2 data. Only flights with turbulence measurements are included.

Flight/Pass	ABL height (km)	u_* (m/s)	T_* (K)	w_* (m/s)	σ_{vector} (m/s)
F3 P1	1.31	0.23	-0.40	1.59	1.02
F3 P2	1.32	0.23	-0.54	1.76	1.11
F3 P3	1.32	0.25	-0.32	1.52	1.00
F3 P4	1.32	0.26	-0.44	1.72	1.12
F4 P1	1.04	0.93	-0.20	1.85	1.95
F4 P2	1.03	0.84	-0.17	1.72	1.78
F4 P3	1.02	0.94	-0.20	1.88	1.97
F4 P4	1.01	0.92	-0.20	1.84	1.93
F5 P1	0.83	0.23	-0.56	1.53	0.99
F5 P2	0.82	0.35	-0.26	1.37	1.02
F5 P3	0.81	0.13	-0.37	1.08	0.68

C. ARISTOTLE JR.

ARISTOTLE Jr. is a 2D array consisting of 23 microphones, labeled M01 to M23. The locations of microphones were constrained to being within 100 ft (30.5 m) of locations already approved by the Bureau of Land Management (BLM) for use by NASA. The footprint of ARISTOTLE Jr. was 600 ft x 125 ft (183 m x 38.1 m). The array was located off track of the flight path. Each microphone was covered with a weather-robust foam windscreen [20]. Figure 3 shows a schematic of the array design with the microphone spacing, which ranged from 25 ft (7.6 m) to 100 ft (30.5 m). The hardware was similar to prior sonic boom measurements [16]. National Instruments data acquisition (DAQ) chassis and 24-bit data acquisition modules were used. GRAS 47AC infrasound-enabled, free-field microphones and GRAS 46AO pressure microphones were used. Despite the difference in microphone type, the angle-of-incidence effects are negligible because the spectral content of the measured booms was below 8 kHz. Figure 4 includes two photos of the setup. Figure 4a) shows the watertight case that housed the DAQ chassis and modules, along with a security stake and steel bike cable, and Figure 4b) shows a portion of the array.

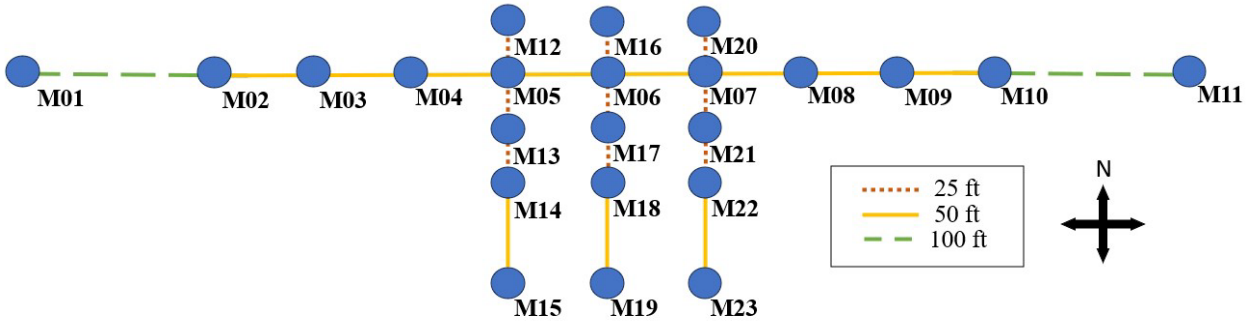

Figure 3. Schematic of ARISTOTLE Jr. The microphone locations are labeled M01 to M23. The spacing between microphones ranged from 25 ft (7.6 m) to 100 ft (30.5 m).

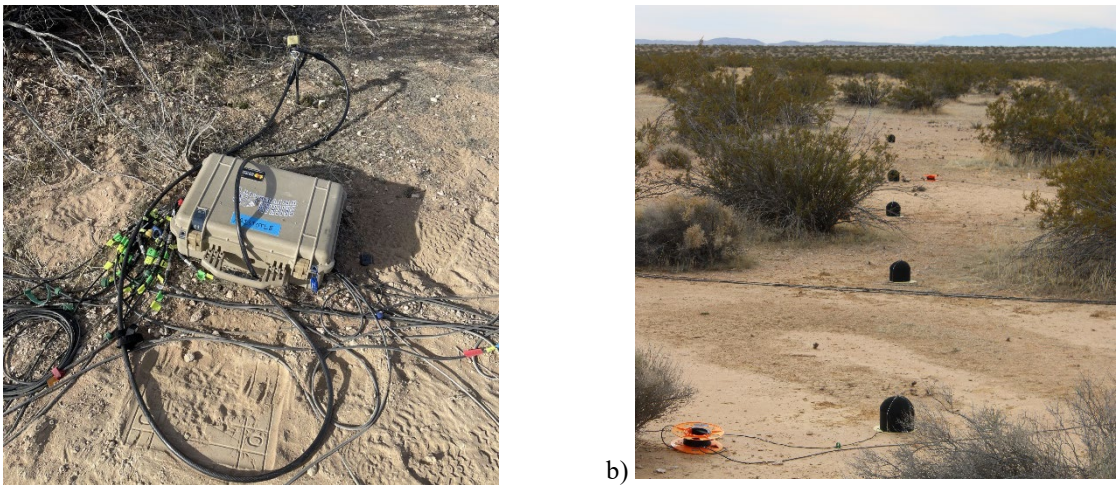

Figure 4. Setup at CarpetDIEM III. a) The DAQ chassis and modules were housed in a watertight case. b) A portion of ARISTOTLE Jr.

IV. Methods

The analysis objectives are to quantify the variability of sonic boom metrics across the array, identify relationships between the variability and conditions during the flight, and use the results to determine the microphone spacing and span required for ARISTOTLE. The six candidate metrics recommended by NASA to quantify the shaped booms were calculated, including A, B, D, and E-weighted Sound Exposure Levels (ASEL, BSEL, DSEL, ESEL), NASA's modification [21] of Stevens Mark VII Perceived Level (PL) [22], and the Indoor Sonic Boom Annoyance Predictor (ISBAP) [23]. PL and BSEL results are included in the paper. PL is shown because it has received the most attention in recent studies [24-26] as it correlates well with human annoyance in the lab [27] and the acoustic requirements for the X-59 were written in terms of PL [24]. BSEL exhibits different statistical behavior than PL because BSEL has a greater emphasis on lower frequencies. Two data correction techniques were used in the analysis. For the 46AO microphones, which have a low-frequency roll off at a higher frequency (~2.5 Hz) than the 47AC (~0.1 Hz) microphones, the proper waveform shape was recovered by enhancing the low-frequency response of the measurement system. Digital pole-shift filtering was used to improve the low-frequency response following the methods of Ref. [28]. Additionally, high-frequency contaminating noise (ambient and instrumentation) was removed using the methods of Ref. [29] to not impact metric calculations that emphasize higher frequencies. Both techniques were employed prior to calculating metrics.

V. Results

CarpetDIEM III encompasses diverse flight and weather conditions, leading to variations in the measurements across different flights and passes. The analysis begins with observed waveforms, followed by PL and BSEL descriptive statistics across the array. The results are then compared with those from CarpetDIEM I and SonicBAT. The discussion includes Signal-to-Noise Ratio (SNR) considerations and study limitations, followed by a detailed analysis of six booms. Waveforms, spectra, and PL across the array are examined for the six examples. Additionally, an analysis of microphones with 25 ft spacing provides insights into array design. Finally, implications are explored for the array design to measure supersonic noise signatures from the X-59 aircraft.

A. Waveforms

The waveform shapes for each microphone in ARISTOTLE Jr. are similar for a given boom, but the shapes vary across flights and passes. An overview of the observed waveforms is given in Figure 5 for each flight and pass for Microphone 01 (M01). For instance, Figure 5a) shows waveforms measured at M01 for the three passes of Flight 1. Flight 4, shown in Figure 5d), has four passes while the other flights have three passes. Waveforms from Flights 1, 3, and 5, which have lower wind speeds in Figure 2c), show turbulent spiking and rounding. The maneuver for Flights 1 and 5 was a supersonic cruise while the maneuver for Flight 3 was a climbing acceleration. Waveforms from Flights 2 and 4, which both had a supersonic cruise maneuver, have more unique waveform shapes. The waveforms have

lower amplitudes and several have a longer duration, which suggests the array may have been in the shadow zone for these flights. The waveforms appear similar to pressure signatures likely in a shadow zone as discussed in Ref. [30] Figure 4. The ground wind speeds were higher for these flights, but the unique waveforms shapes may be a result of the array being in the shadow zone. Ref. [17] includes the PCBoom sonic boom carpet footprint for Flight 5 Passes 1 and 2, but the footprints for Flight 2 and 4 are not shown. Future work includes running PCBoom to investigate the location of the array relative to the footprint.

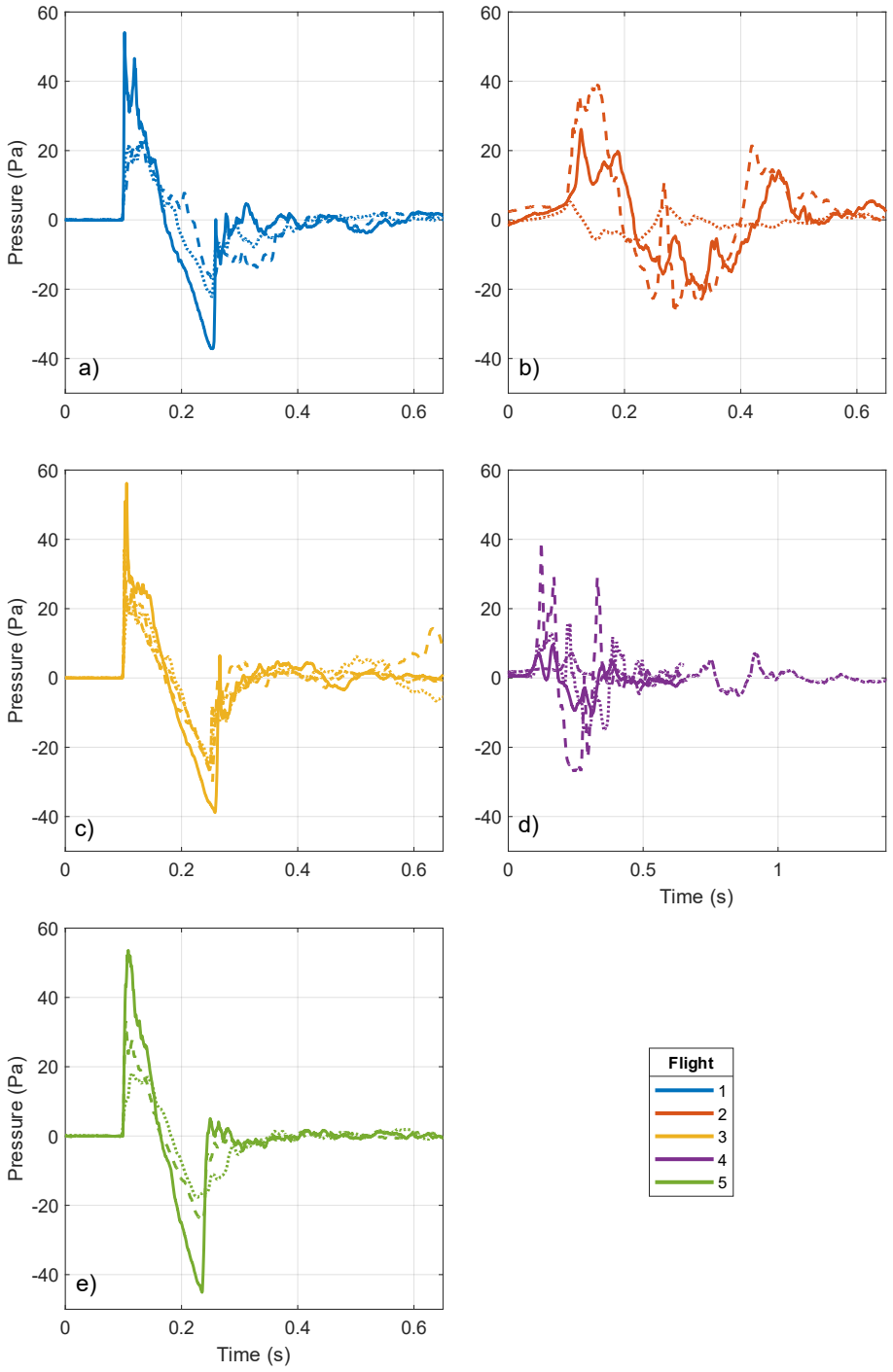

Figure 5. Waveforms for M01 for a) Flight 1, b) Flight 2, c) Flight 3, d) Flight 4, and e) Flight 5. The line style is different for each pass in a given flight.

B. PL and BSEL Ranges and Standard Deviations

Table 3 presents PL and BSEL means and ranges, PL standard deviations, σ_{PL}, and BSEL standard deviations, σ_{BSEL}, across the 23-microphone array for each flight and pass. Figure 6a) illustrates PL and BSEL ranges and Figure 6b) illustrates σ_{PL} and σ_{BSEL}. The color denotes flight number. The boom from Flight 4 Pass 2 has the lowest mean

PL but the highest PL range and σ_{PL}. A single outlier results in the high PL range and σ_{PL}. Conversely, the boom with the largest mean PL is from Flight 5 Pass 1, which also has the next highest PL range and σ_{PL}. The ranges for BSEL are smaller than the ranges for PL, and Flight 4 Pass 3 and Flight 5 Pass 1 have the largest BSEL ranges. Flight 4 has higher wind speeds, whereas Flight 5 has lower wind speeds. The mean PL for Flight 1 Pass 3 is representative of the overall measurement, but it has a low PL range and σ_{PL}. Typically, the mean PL is greater than the mean BSEL across the array. For each flight and pass, the PL range and σ_{PL} are greater than the BSEL range and σ_{BSEL}.

Table 3. PL and BSEL descriptive statistics. The values are calculated across the array for each flight and pass.

Flight/Pass	Mean PL (dB)	PL range (dB)	σ_{PL} (dB)	Mean BSEL (dB)	BSEL range (dB)	σ_{BSEL} (dB)
F1 P1	98.0	5.9	1.5	93.6	4.3	1.2
F1 P2	84.4	4.5	1.2	82.5	3.8	1.0
F1 P3	84.4	4.0	0.9	82.2	2.8	0.7
F2 P1	84.1	6.6	1.5	82.4	6.0	1.4
F2 P2	91.1	4.5	1.1	88.2	3.3	0.8
F2 P3	64.8	6.6	1.6	69.6	3.0	0.7
F3 P1	93.7	8.7	2.4	90.1	7.0	2.1
F3 P2	92.7	9.2	1.9	89.2	7.5	1.5
F3 P3	87.7	7.0	1.8	84.9	6.0	1.6
F3 P4	86.9	9.0	1.8	84.5	7.5	1.5
F4 P1	69.6	4.5	1.1	73.3	2.6	0.8
F4 P2	59.1	17.2	2.8	72.1	2.3	0.5
F4 P3	86.7	9.2	2.3	85.9	8.1	1.8
F4 P4	85.0	4.6	1.1	84.2	3.6	0.9
F5 P1	100.3	13.3	3.4	94.8	8.7	2.4
F5 P2	89.0	5.0	1.2	85.7	4.0	0.9
F5 P3	79.4	3.6	1.0	79.1	2.8	0.8

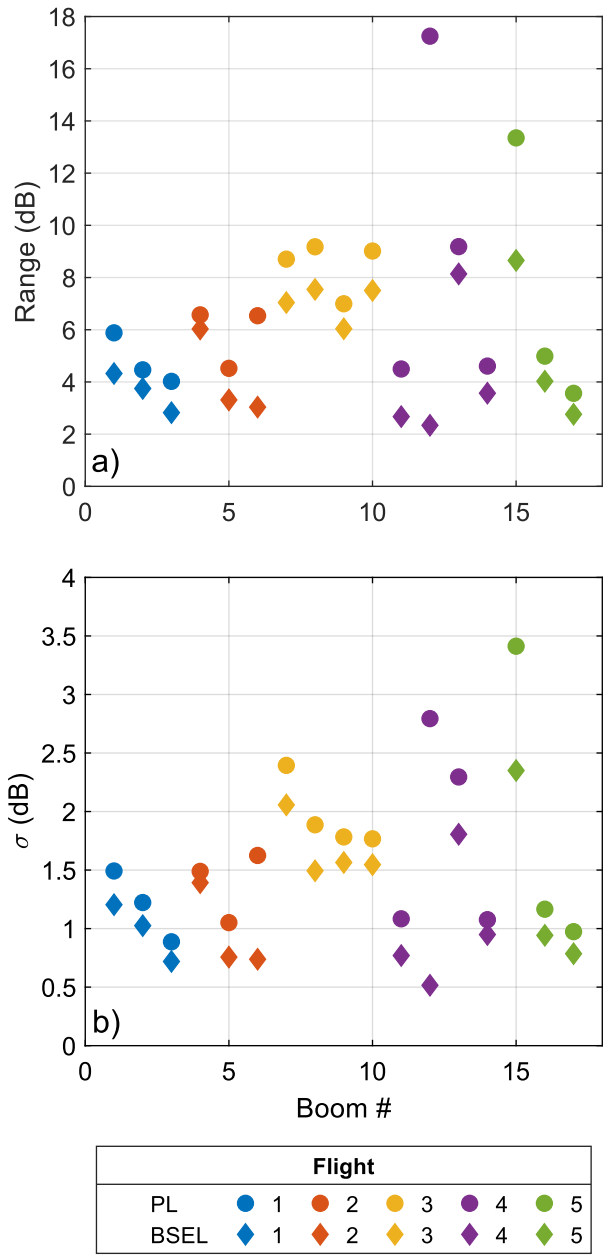

Figure 6. Ranges and standard deviations of PL and BSEL across the array for each boom. PL is denoted with circular marker and BSEL is denoted with diamond markers. a) PL and BSEL ranges. b) σ_{PL} and σ_{BSEL}.

CarpetDIEM III results are comparable to CarpetDIEM I results. In CarpetDIEM I, a seven-microphone turbulence array was deployed and recorded 23 booms [16]. The microphone spacing ranged from 50 ft (15.2 m) to 100 ft (30.5 m), with the linear array spanning 400 ft (122 m). Table 4 includes a comparison of CarpetDIEM III and I statistics. When averaging the values across all flights and passes for CarpetDIEM III at ARISTOTLE Jr., the mean PL is 84.5 dB, the mean of the PL range is 7.3 dB, and the mean of σ_{PL} is 1.7 dB. The mean BSEL for the measurement campaign is 83.7 dB, the mean BSEL range is 4.9 dB, and the mean σ_{BSEL} is 1.2 dB. For CarpetDIEM I, the mean PL across the turbulence array was 103.7 dB, the mean PL range was 7.4 dB and the mean σ_{PL} was 2.8 dB. Although the booms had a larger PL on average, the range of PL and σ_{PL} are comparable to CarpetDIEM III. Further details and explanations of the CarpetDIEM I turbulence array will be included in a forthcoming paper [31, submitted (2025)].

Table 4. Comparison of PL descriptive statistics for CarpetDIEM III and I. The values are averaged across all flights and passes.

Measurement Campaign	Array	Mean PL (dB)	Mean PL range (dB)	Mean σ_{PL} (dB)
CarpetDIEM III	ARISTOTLE Jr.	84.5	7.3	1.7
CarpetDIEM I	Turbulence array	103.7	7.4	2.8

For SonicBAT, two cross arrays, designated as the secondary and tertiary arrays, were deployed. Each array consisted of eight microphones with 100 ft (30.5 m) spacing, and the cross array spanned 300 ft x 300 ft (91.4 m x 91.4 m). Unlike CarpetDIEM I and III, where PL statistics are analyzed per boom, SonicBAT reported the mean PL and mean standard deviation averaged over all measurements. The values are included in Table 5. The mean PL was 101.3 dB for the secondary array and 100.3 dB for the tertiary array, with corresponding mean standard deviations of 4.1 dB and 4.5 dB. The PL standard deviation for all measurements for CarpetDIEM III is 10.9 dB, which is greater than that of SonicBAT. Given the variability in flight trajectories and weather conditions during CarpetDIEM III, booms were not expected to have the same PL.

Table 5. Comparison of PL descriptive statistics for CarpetDIEM III and SonicBAT. The values are averaged over all measurements.

Measurement Campaign	Array	Mean PL (dB)	Mean standard deviation (dB)
CarpetDIEM III	ARISTOTLE Jr.	84.5	10.9
SonicBAT	Secondary array	101.3	4.1
SonicBAT	Tertiary array	100.3	4.5

The mean SNR for PL and BSEL for CarpetDIEM III is included in Figure 7. The SNR compares the level of the boom after ambient noise has been removed with the ambient level. The marker represents the average SNR, while the error bars represent the SNR range. The days with stronger wind speeds correspond to lower average SNR values. Specifically, Figure 7a) shows Flight 2 Pass 3, Flight 4 Pass 1, and Flight 4 Pass 2 have an average PL SNR around 0 dB, and several measurements have a negative SNR. In these cases, the ambient PL exceeded the boom PL, making it difficult to distinguish the boom from the ambient noise. To identify the booms in these recordings, cross-correlation was used. This difficulty in differentiating booms from noise is an important consideration for X-59 testing [32], due to the low loudness level (PL of 75 dB) of supersonic signatures expected from that vehicle [33]. The BSEL SNR, shown in Figure 7b), follows similar trends as PL SNR, but the BSEL SNR values are greater.

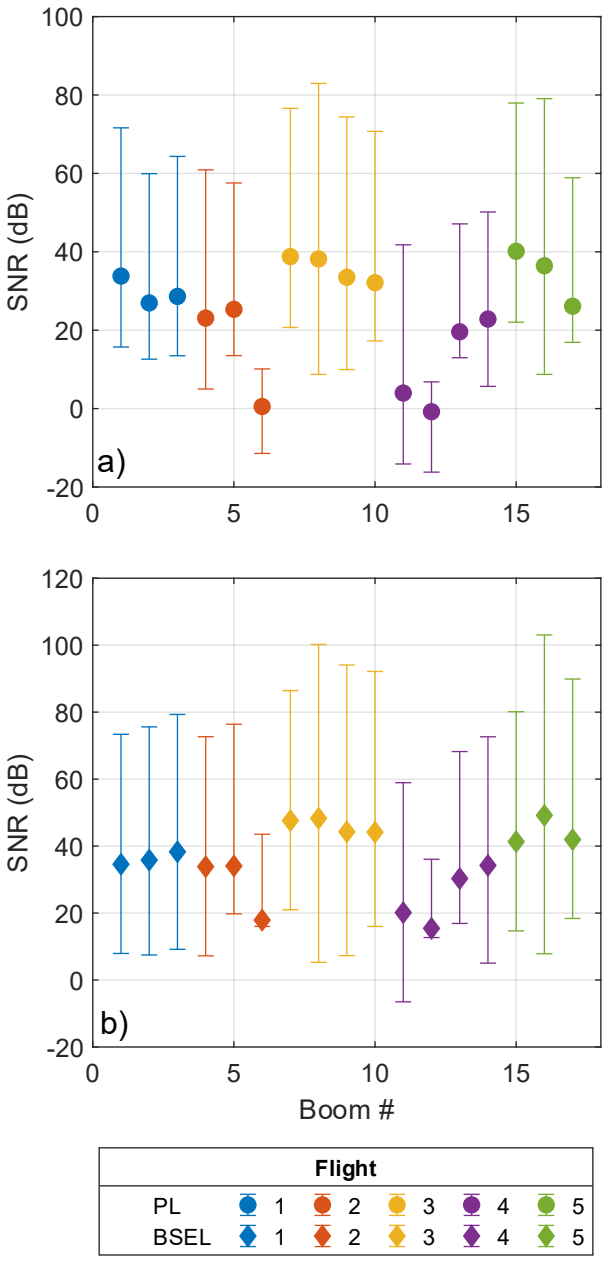

Figure 7. Mean SNR for each boom. The marker color denotes flight, and the error bars represent the range of SNR for each boom. a) PL SNR. b) BSEL SNR.

C. Examples

Six of the seventeen booms are examined in greater detail to better understand how heading, maneuver, and weather conditions affect the waveforms, spectra, and resulting PL across the array. The six examples include two with a small PL range and σ_{PL}, two with a medium PL range and σ_{PL}, and two with a large PL range and σ_{PL}. The discussion begins with waveforms and spectra, followed by the PL across the array. Both the measured and ambient spectra are shown, and the ambient noise was removed prior to calculating metrics.

The waveforms and spectra for two cases with low variability are shown in Figure 8. Flight 5 Pass 3 is shown in Figure 8a) and b) and Flight 1 Pass 3 is shown in Figure 8c) and d). The measured waveform and spectrum for each microphone in the array are shown in color, and the ambient spectrum is shown for each microphone in gray. The bold line is for M01, which is the same microphone whose waveform is displayed in Figure 5. For both cases, there is

visible turbulent peaking in the waveforms. The detrend function in MATLAB [34] is applied to the waveforms, but a residual DC offset preceding the shock remains. Figure 8b) and Figure 8d) show the high-frequency content is similar for all microphones for each boom. One of the microphones has a higher noise floor in the ambient spectrum, which is a result of intermittent cable noise. However, this does not impact the metrics because the noise is removed prior to metric calculations.

Two examples of medium variability are shown in Figure 9. Figure 9a) and b) include Flight 3 Pass 3 and Figure 9c) and d) include Flight 2 Pass 1. For Flight 2 Pass 1, there were some low-frequency correlated acoustic signatures immediately preceding the boom, so a 650 ms segment of ambient a couple of seconds prior to the boom was used for the ambient removal. The waveforms shapes are different between the two booms. The first, in Figure 9a), has some turbulent spiking in the waveform and the microphones have different high frequency content. For the second example, the waveform shape is different from the typical N-wave. There are small differences in the spectra at frequencies under 100 Hz, but the high-frequency content is similar.

The final examples are for high variability. Flight 5 Pass 1 is shown in Figure 10a) and b). Turbulent spiking is visible in the waveforms and manifested in the high frequency variation in the spectra. The spectra begin to diverge around 50 Hz, and the differences between microphones are greater than 25 dB at high frequencies. Flight 4 Pass 2 is shown in Figure 10c) and d). This boom is low amplitude and difficult to separate from the ambient noise. The ambient spectra are higher at low frequencies compared to previous booms. One microphone, M08, has a different waveform shape for the first half of the boom. The pressure drops to around -25 Pa at 0.4 s instead of following the same trend as the other microphones in the array. There is a clear difference in pressure due to wind or acoustics for M08 for this boom, but there is no compelling evidence to exclude this recording as playback with high-quality headphones confirms the recording has an audible boom and there are no issues with this microphone in other recordings.

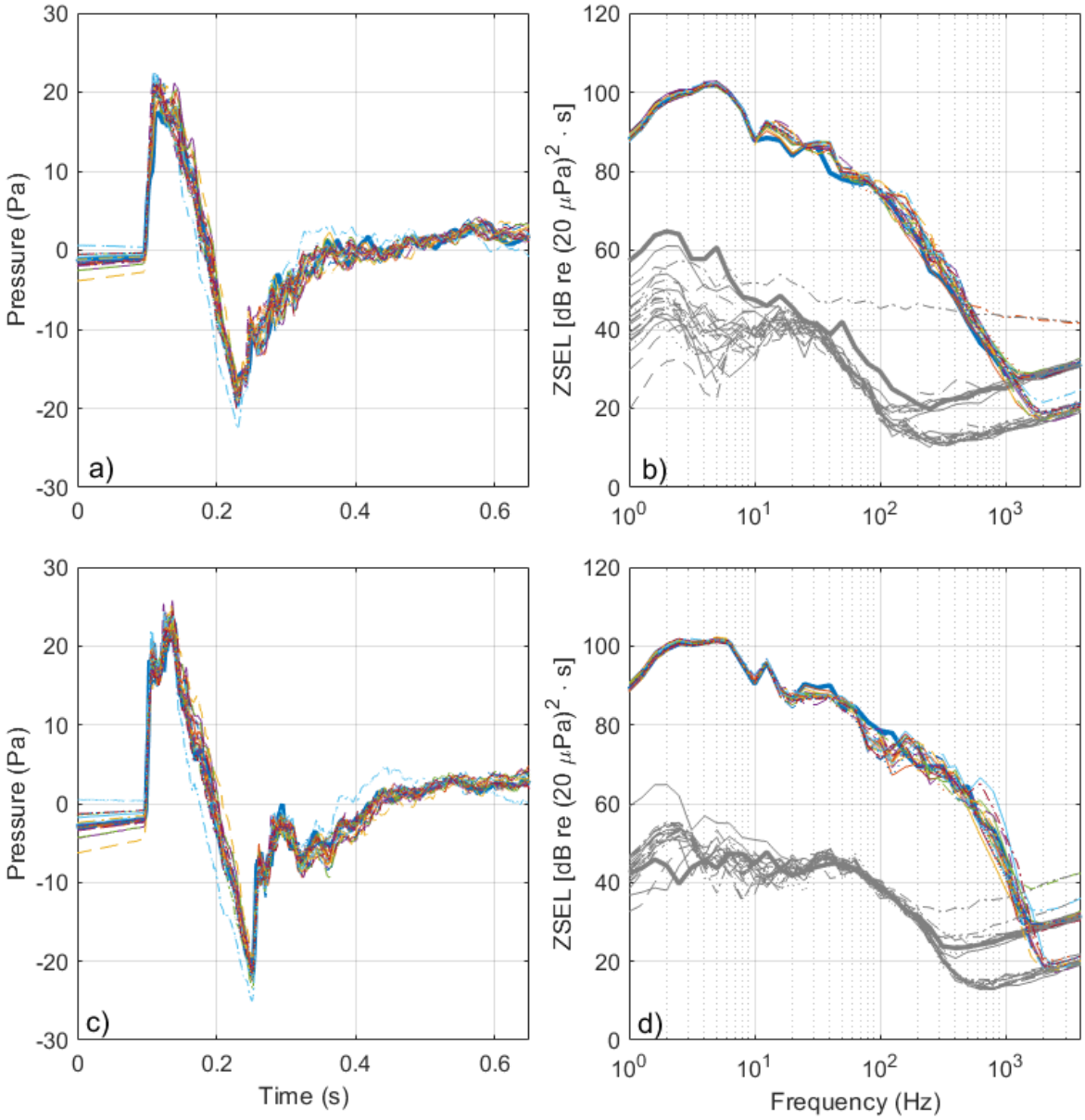

Figure 8. Two overflights with low variability. a) and b) Flight 5 Pass 3. c) and d) Flight 1 Pass 3.

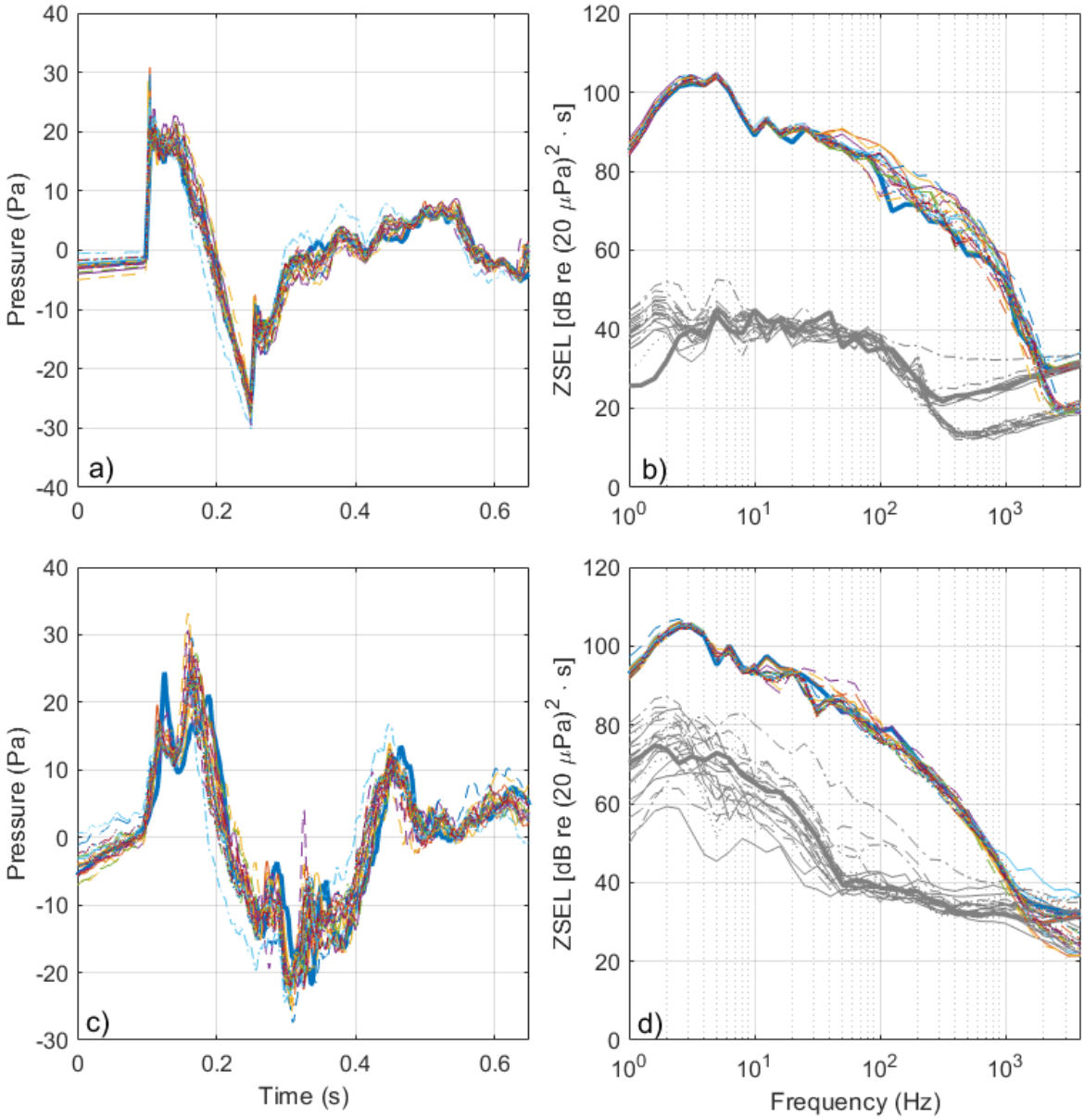

Figure 9. Two overflights with medium variability. a) and b) Flight 3 Pass 3. c) and d) Flight 2 Pass 1.

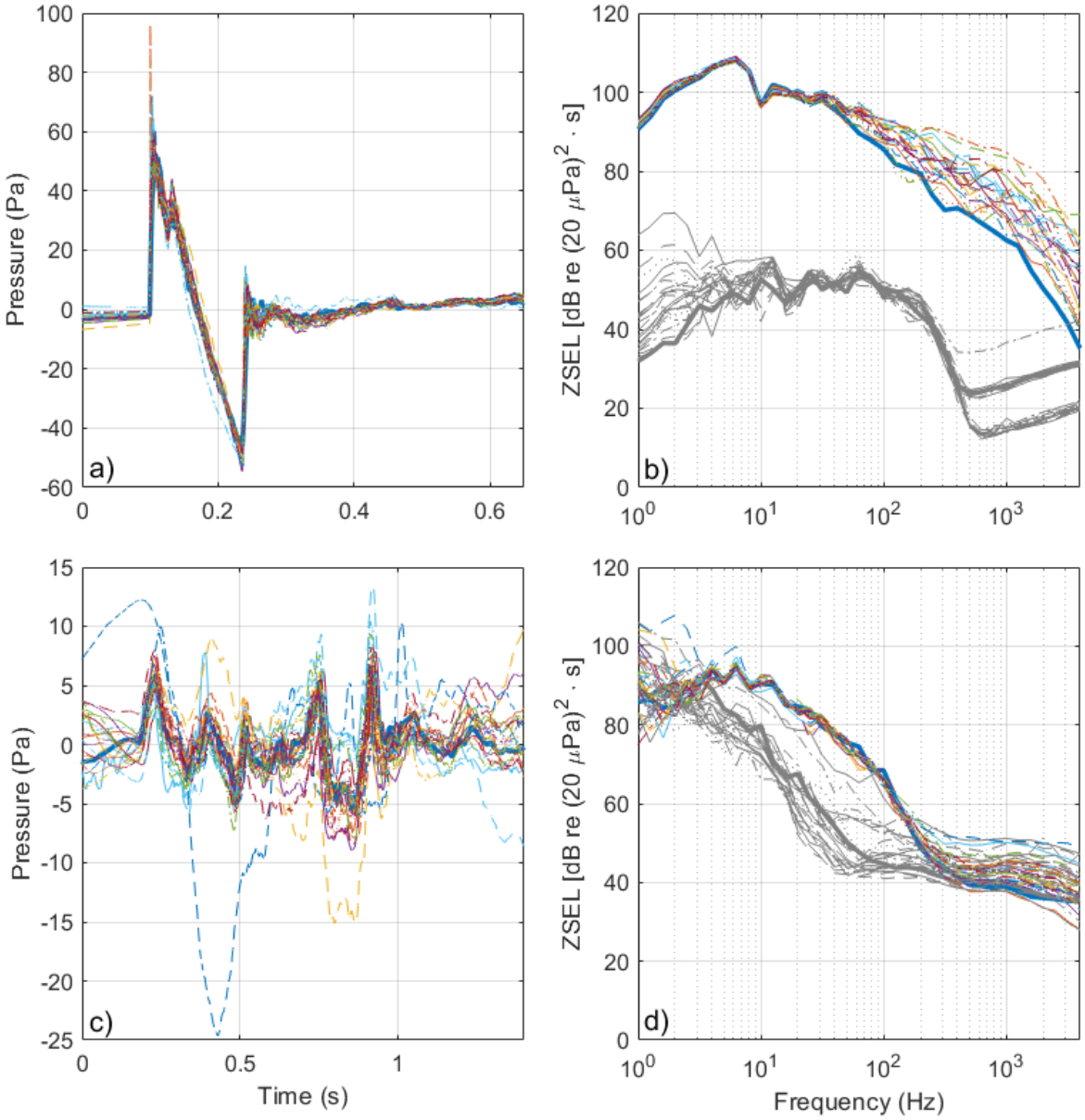

Figure 10. Two overflights with high variability. a) and b) Flight 5 Pass. c) and d) Flight 4 Pass 2.

The PL across the array for each boom is shown in Figure 11. The location of each marker represents the physical location of the microphones in the array. The marker color denotes the PL relative to the mean PL across the array for that flight. A standard scale of -7 to 7 dB is used for all booms, so the colors can be compared across flights. The PL for M08 was 10.5 dB greater than the mean for Figure 11f), so the PL relative to the mean is included as an annotation. The marker size denotes the absolute value of PL relative to the mean PL, so the marker is smallest for a PL equal to the mean. The size is also standardized so it can be compared across booms. Heading information is also included. The arrow in the lower-left signifies the heading, which is either northbound, eastbound, or westbound. The maneuver, either a supersonic cruise or a climbing acceleration, is noted in the lower-right. Note that the axes scaling in Figure 11 is not one to one. The array spanned 600 ft × 125 ft (183 m × 38.1 m), so the figure aspect ratio has been adjusted to more clearly visualize the differences in PL across the array.

The distance over which the maximum PL range occurs for each of the six examples is listed in Table 6. There is not a clear correlation between distance and maximum PL variation. Flight 5 Pass 3, shown in Figure 11a), and Flight

1 Pass 3, shown in Figure 11b), both were for supersonic cruise flights. Both booms had a PL range of around 4 dB, but the distance over which this range occurs is different. The maximum range occurred over 351 ft (107 m) for Flight 5 Pass 3, while it occurred over only 71 ft (21.6 m) for Flight 1 Pass 3. The examples for medium variability were both for climbing acceleration flights. Flight 3 Pass 3, included in Figure 11c), and Flight 2 Pass 1, included in Figure 11d), has a PL range around 7 dB. The distances between microphones for the range are similar for these booms, 350 ft (107 m) and 364 ft (111 m), respectively. The high variability examples are for different maneuvers. Flight 5 Pass 1, shown in Figure 11e), is for a supersonic cruise flight and has high amplitudes and low wind. The range of 13.3 dB occurred over 301 ft (91.7 m). In contrast, Flight 4 Pass 2, shown in Figure 11f), is for a climbing acceleration flight and has low amplitudes and high wind. The PL range of 17.2 dB occurs over 100 ft (30.5 m).

To measure the variability of metrics due to atmospheric turbulence, the array must be large enough to capture the length scale associated with metric variation. Figure 11 illustrates trends in PL. For example, Figure 11e) shows quieter levels on the southwest side of the array and louder levels on the northeast side. Each of the 17 booms also have regions of loud and quiet; however, the absence of repeating regions, i.e. the characteristic wavelength in metric value cannot be observed, suggests that the ARISTOTLE Jr. array aperture is not large enough.

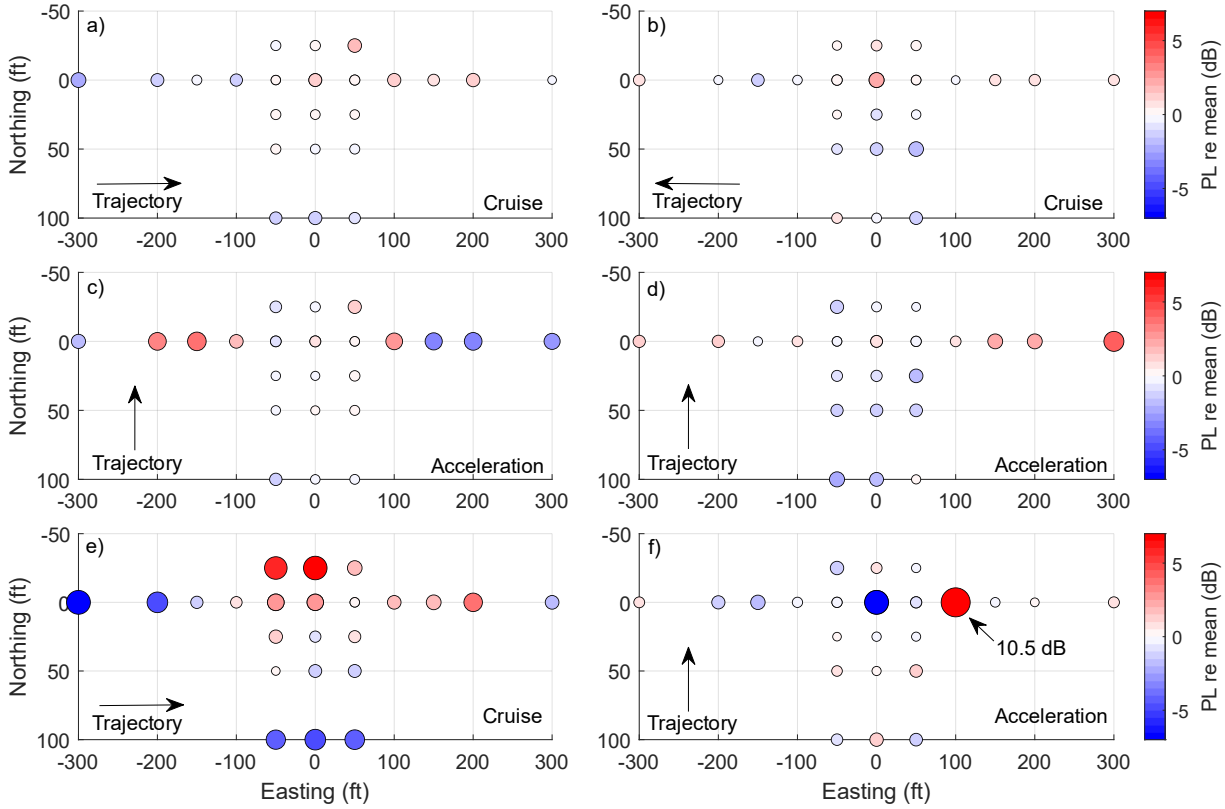

Figure 11. PL across the array. a) Flight 5 Pass 3. b) Flight 1 Pass 3. c) Flight 3 Pass 3. d) Flight 2 Pass 1. e) Flight 5 Pass 1. f) Flight 4 Pass 2.

Table 6. Distance over which the maximum PL range occurred for each flight and pass.

Flight/Pass	PL range (dB)	Distance for maximum PL range (ft)
F1 P1	5.9	224
F1 P2	4.5	202
F1 P3	4.0	71
F2 P1	6.5	364
F2 P2	4.5	600
F2 P3	6.6	180
F3 P1	8.7	351
F3 P2	9.2	600

F3 P3	7.0	350
F3 P4	9.0	269
F4 P1	4.5	112
F4 P2	17.2	100
F4 P3	9.2	500
F4 P4	4.6	316
F5 P1	13.3	301
F5 P2	5.0	500
F5 P3	3.6	351

The measured variability for CarpetDIEM III is informative for array design. Of the 17 booms, the maximum PL range was observed over both dimensions of the array for 11 booms. The second dimension only extended 125 ft (38.1 m) beyond the linear array, but substantial variations in PL were measured over that distance. This supports the need to use a 2D array for future measurements to capture the variability due to atmospheric turbulence.

To investigate the impact of 25 ft (7.6 m) spacing, a leave-one-out analysis is conducted for the three 25 ft (7.6 m) spacing vertical arrays. The 25 ft (7.6 m) spacing covers a total of 75 ft (22.9 m). The mean PL with four microphones is compared to the mean using three microphones. Because the three vertical arrays are separated by 50 ft (15.2 m), the analysis is performed for each array separately. The maximum difference in PL mean out of the three arrays is included in Table 7. The mean PL from the leave-one-out analysis is subtracted from the original mean PL of the vertical array, so a positive value indicates that the original range is larger than the leave-one-out analysis. For many booms, the magnitude of the maximum difference in mean PL by leaving out one microphone with 25 ft (7.6 m) spacing is around 1 dB. The analysis is repeated for the PL range. Again, the maximum difference in range from leaving out on microphone is reported in Table 7. The average change of the magnitude of PL range when a microphone is excluded from a 75 ft (22.9 m) array is 2.1 dB and the maximum difference is 6.3 dB. The leave-one-out analysis is limited to one dimension because the three vertical arrays were separated by 50 ft (15.2 m) in the east/west direction. It is also limited to 75 ft (22.9 m) in the north/south direction because only four microphones have 25 ft (7.6 m) spacing in each vertical array. Although the analysis was limited, the results suggest that there are cases where a fine resolution is needed to capture the variability of PL.

Table 7. Leave-one-out analysis for 25 ft spacing.

Flight/Pass	Maximum difference in mean PL (dB)	Maximum difference in PL range (dB)
F1 P1	1.0	2.4
F1 P2	1.1	1.9
F1 P3	-0.5	2.9
F2 P1	0.7	1.3
F2 P2	0.4	-0.7
F2 P3	-1.3	-3.1
F3 P1	-0.5	-0.8
F3 P2	0.6	-2.0
F3 P3	0.6	0.9
F3 P4	0.4	1.2
F4 P1	2.2	2.5
F4 P2	-1.6	6.3
F4 P3	-1.5	1.7
F4 P4	-1.3	1.0
F5 P1	-1.6	5.1
F5 P2	-0.7	1.1
F5 P3	0.4	1.4

D. Implications for X-59

CarpetDIEM III presents several challenges of measuring quiet sonic booms in real-world environments. While the goal of ARISTOTLE Jr. is to prepare to assess the variability of X-59 measurements due to turbulence, ambient noise is another cause of variability. For CarpetDIEM III, many of the low-amplitude booms – around the X-59 target

PL value of 75 dB [33] – are highly variable and contaminated with ambient noise. As discussed in Ref. [29], higher frequencies that are more influential in PL calculations have lower SNR values, which can inflate metrics with contaminating noise. Although removing the contaminating noise is necessary to calculate the PL of the booms, the calculation procedure is sensitive to selecting an appropriate lowpass filter cutoff frequency. For these low-amplitude booms, the variability across ARISTOTLE Jr. may not be caused by turbulence-induced variation but rather variations in ambient noise (e.g., rustling of sage brush or whistling of wind through branches). Flight 4 Pass 2, shown in Figure 11f), is one example. The measurement with the smallest PL, at location (0,0) ft, has a cutoff frequency of 80 Hz. The rest of the measurements have a cutoff frequency between 160 Hz and 400 Hz for this boom. This frequency range is smaller than the typical cutoff frequency required to estimate the PL of the boom within 1 dB (see Table III in Ref. [29]) and 80 Hz to 400 Hz falls within the peak of the specific loudness for the predicted X-59 boom. Thus, assessments of low-amplitude booms influenced by contaminating noise may be as variable as high-amplitude booms with large SNR affected by turbulence focusing. This demonstrates a challenge of measuring low booms in environments with relatively high-amplitude, nonstationary noise, such as the ambient noise in an urban environment, which may be the case for community testing. This also demonstrates the importance of array measurements to further study the challenge prior to community testing of X-59.

E. ARISTOTLE Design

CarpetDIEM III results are used to determine the size of array and microphone spacing required for ARISTOTLE to measure the variability of sonic boom metrics due to atmospheric turbulence. CarpetDIEM III results suggest that 600 ft (183 m) is not large enough to capture the length scales associated with metric variation. The measured difference in PL across 25 ft (7.6 m) for CarpetDIEM III is relatively small (an average of 0.8 dB, with five instances where the variability was greater than 3 dB), which is consistent with the literature [3]. However, results from the limited leave-one-out analysis indicate that in some cases, removing one microphone can result in a notable difference in PL range. This suggests that there are cases where fine resolution is needed. To further investigate the spacing, a portion of ARISTOTLE will have 25 ft (7.6 m) spacing in two dimensions to ensure that the resolution is fine enough and to study the error associated with a coarser measurement resolution and data interpolation.

Based on these results, the proposed design for ARISTOTLE is shown in Figure 12. The cross array will span 1,000 ft x 1,000 ft (305 m x 305 m), which is expected to be adequate to capture the 2D metric variation length scale and satisfy logistical constraints. The arms constructing the cross will have 50 ft (15.2 m) spacing, and 25 (5 x 5) microphones will be placed near the center to create a grid with 25 ft (7.6 m) spacing. A total of 61 microphones will be used. This array will be used to measure the variability due to atmospheric turbulence of shaped booms from the X-59 in preparation for community testing.

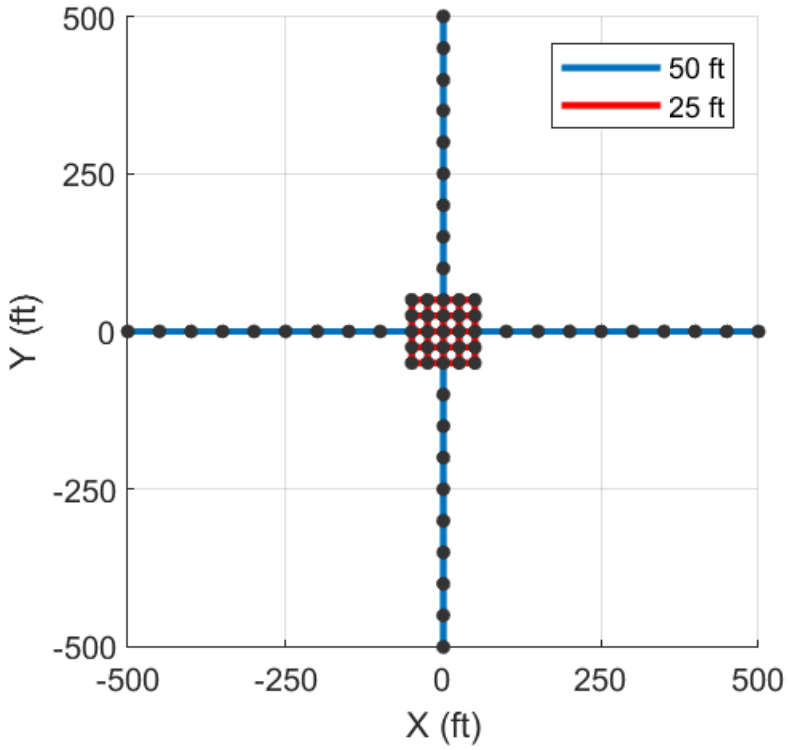

Figure 12. ARISTOTLE design. The microphones are denoted by points and spacing is denoted by color.

VI. Conclusion

The CarpetDIEM III measurement campaign was an extensive effort that has already yielded valuable information about the 2D variation in sonic boom metric levels due to turbulence. ARISTOTLE Jr., a 2D, 23-microphone array, measured 17 booms at CarpetDIEM III. The range and standard deviation across the array are greater for PL than BSEL, and there is considerable pass-to-pass variation. The average range of PL across the array for CarpetDIEM III is 7.3 dB and the average σ_{PL} is 1.7 dB. The most noticeable difference in weather conditions between flights was the wind speed. The maximum PL range occurred on a day with higher wind speeds, but the maximum σ_{PL} and other large PL ranges occurred on days with lower wind speeds. CarpetDIEM III demonstrated that high variability in PL can be caused by ambient noise or atmospheric turbulence. Because the variability of metrics differs in the north/south and east/west directions, a 2D ARISTOTLE array is needed to measure the variability. The full ARISTOTLE array will consist of 61 microphones that span 1,000 ft x 1,000 ft (305 m x 305 m). The array will be tested with booms from an F-15 during the Phase 2 Dry Run campaign. ARISTOTLE will be used to measure the variability of metrics from X-59 supersonic signatures due to atmospheric turbulence.

References

[1] Rathsam, J., Coen, P., Loubeau, A., Ozoroski, L., and Shah, G., "Scope and Goals of NASA's Quesst Community Test Campaign with the X-59 Aircraft," 14th ICBEN Congress on Noise as a Public Health Problem, 2023.

[2] NASA, "NASA Quesst Mission Webpage," 2024. Retrieved 22 August 2024. https://www.nasa.gov/X59

[3] Maglieri, D. J., Bobbitt, P. J., Plotkin, K. J., Shepherd, K. P., Coen, P. G., and Richwine, D. M., "Sonic Boom: Six Decades of Research," NASA/SP-2014-622, 2014.

[4] Yamashita, H., and Obayashi, S., "Sonic Boom Variability Due to Homogeneous Atmospheric Turbulence," *Journal of Aircraft*, Vol. 46, No. 6, 2009, pp. 1886–1893. https://doi.org/10.2514/1.40215

[5] Raspet, R., Bass, H. E., Yao, L., Boulanger, P., and McBride, W. E., "Statistical and Numerical Study of the Relationship between Turbulence and Sonic Boom Characteristics," *The Journal of the Acoustical Society of America*, Vol. 96, No. 6, 1994, pp. 3621–3626. https://doi.org/10.1121/1.410579

[6] Lipkens, B., and Blanc-Benon, P., "Effect of Turbulence on the Risetime of Sonic Booms and Spark Generated N Waves," *Journal of The Acoustical Society of America*, Vol. 112, 2002, p. 2215. https://doi.org/10.1121/1.4778735

[7] Pierce, A. D., "Statistical Theory of Atmospheric Turbulence Effects on Sonic-Boom Rise Times," *The Journal of the Acoustical Society of America,* Vol. 49, No. 3B, 1971, pp. 906–924. https://doi.org/10.1121/1.1912431

[8] Stout, T. A., "Simulation of N-Wave and Shaped Supersonic Signature Turbulent Variations," Ph.D. dissertation. The Pennsylvania State University, 2018.

[9] Stout, T. A., Sparrow, V. W., and Blanc-Benon, P., "Evaluation of Numerical Predictions of Sonic Boom Level Variability Due to Atmospheric Turbulence," *The Journal of the Acoustical Society of America*, Vol. 149, No. 5, 2021, pp. 3250–3260. https://doi.org/10.1121/10.0004985

[10] Bradley, K. A., Hobbs, C. M., Wilmer, C. B., Sparrow, V. W., Stout, T. A., Morgenstern, J. M., Underwood, K. H., Maglieri, D. J., Cowart, R. A., Collmar, M. T., Shen, H., and Blanc-Benon, P., "Sonic Booms in Atmospheric Turbulence (SonicBAT): The Influence of Turbulence on Shaped Sonic Booms," NASA/CR–2020–220509, 2020.

[11] Downs, R., Barzach, M., Doebler, W., Parker, P. A., Loubeau, A., and Lonzaga, J. B., "Turbulence Effects on Shaped Booms: Propagation Simulations Using KZKFourier," *The Journal of the Acoustical Society of America*, Vol. 153, No. 3_supplement, 2023, pp. A326–A326. https://doi.org/10.1121/10.0019017

[12] Lipkens, B., and Blackstock, D. T., "Model Experiment to Study Sonic Boom Propagation through Turbulence. Part I: General Results," *The Journal of the Acoustical Society of America*, Vol. 103, No. 1, 1998, pp. 148–158. https://doi.org/10.1121/1.421114

[13] Ollivier, S., and Blanc-Benon, P., "Model Experiments to Study Acoustic N-Wave Propagation Through Turbulent Media," 10th AIAA/CEAS Aeroacoustics Conference, *American Institute of Aeronautics and Astronautics*, 2004. https://doi.org/doi:10.2514/6.2004-2921

[14] Salze, E., Ollivier, S., Jondeau, E., and Blanc-Benon, P., "Acoustical Propagation of Weak Shockwaves Into a Shadow Zone With Turbulence: Laboratory-Scale Experiment," AIAA 2024-3186. *30th AIAA/CEAS Aeroacoustics Conference,* 2024. https://doi.org/10.2514/6.2024-3186

[15] Stout, T. A., and Sparrow, V. W., "Three-Dimensional Simulation of Shaped Sonic Boom Signature Loudness Variations Due to Atmospheric Turbulence," *25th AIAA/CEAS Aeroacoustics Conference*, American Institute of Aeronautics and Astronautics, 2019. https://doi.org/doi:10.2514/6.2019-2562

[16] Durrant, J. T., Gee, K. L., Anderson, M. C., Mathews, L. T., Rasband, R. D., Novakovich, D. J., Loubeau, A., and Doebler, W. J., "An Overview of Brigham Young University's Participation in NASA's CarpetDIEM Campaign," *Proceedings of Meetings on Acoustics*, Vol. 43, No. 1, 2022, p. 045002. https://doi.org/10.1121/2.0001589

[17] Carpenter, F. L., Hantsche, L. J., Cliatt, L. J., Haering, E. A., "Supersonic Flight Testing to Assess Ground Recording Systems for NASA's Low Boom Flight Demonstrator," AIAA 2025-0194. *AIAA SCITECH 2025 Forum*, 2025. https://doi.org/10.2514/6.2025-0194

[18] Saha, S., Moorthi, S., Wu, X., Wang, J., Nadiga, S., Tripp, P., Behringer, D., Hou, Y.-T., Chuang, H., Iredell, M., Ek, M., Meng, J., Yang, R., Mendez, M. P., van den Dool, H., Zhang, Q., Wang, W., Chen, M., and Becker, E., "The NCEP Climate Forecast System Version 2," *Journal of Climate*, Vol. 27, No. 6, 2014, pp. 2185–2208. https://doi.org/10.1175/JCLI-D-12-00823.1

[19] Doebler, W., and Loubeau, A., "A Procedure for Obtaining Forecast Turbulence Parameters in the Atmospheric Boundary Layer for Acoustic Propagation," *The Journal of the Acoustical Society of America*, Vol. 154, No. 4_supplement, 2023, pp. A147–A147, 2023. https://doi.org/10.1121/10.0023075

[20] Anderson, M. C., Gee, K. L., Novakovich, D. J., Rasband, R. D., Mathews, L. T., Durrant, J. T., Leete, K. M., and Loubeau, A., "High-Fidelity Sonic Boom Measurements Using Weather-Robust Measurement Equipment," *Proceedings of Meetings on Acoustics*, Vol. 39, No. 1, 2022, p. 040005, 2019. https://doi.org/10.1121/2.0001578

[21] Shepherd, K. P., and Sullivan, B. M., "A Loudness Calculation Procedure Applied to Shaped Sonic Booms," NASA-TP-3134, 1991.

[22] Stevens, S. S., "Perceived Level of Noise by Mark VII and Decibels (E)," *The Journal of the Acoustical Society of America*, Vol. 51, No. 2B, 1972, pp. 575–601, 1972. https://doi.org/10.1121/1.1912880

[23] Loubeau, A., and Page, J., "Human Perception of Sonic Booms from Supersonic Aircraft Advances in Human Response Research Will Help Pave The Way for a New Era of Commercial Supersonic Flight," *Acoustics Today*, Vol 15, Issue 3, 2018.

[24] Lee, J., Rathsam, J., and Wilson, A., "Bayesian Statistical Models for Community Annoyance Survey Data," *The Journal of the Acoustical Society of America*, Vol. 147, No. 4, pp. 2222–2234, 2020. https://doi.org/10.1121/10.0001021

[25] Doebler, W. J., and Loubeau, A., "Estimating the Noise Dose Range of the NASA X-59 Aircraft in Supersonic Cruise Using PCBoom Propagation Simulations," *JASA Express Letters*, Vol. 3, No. 5, p. 053601, 2023. https://doi.org/10.1121/10.0019501

[26] Vaughn, A. B., and Christian, A. W., "A Generalized Cumulative Noise Exposure Metric for Community Response Analysis," *The Journal of the Acoustical Society of America*, Vol. 155, No. 2, pp. 1272–1284, 2024. https://doi.org/10.1121/10.0024765

[27] Rathsam, J., Klos, J., Loubeau, A., Carr, D. J., and Davies, P. "Effects of chair vibration on indoor annoyance ratings of sonic booms," *The Journal of the Acoustical Society of America*, 143(1), 489–499, 2018. https://doi.org/10.1121/1.5019465

[28] Rasband, R. D., Gee, K. L., Gabrielson, T. B., and Loubeau, A., "Improving Low-Frequency Response of Sonic Boom Measurements through Digital Filtering," *JASA Express Letters*, Vol. 3, No. 1, p. 014802, 2023. https://doi.org/10.1121/10.0016751

[29] Anderson, M. C., Gee, K. L., Durrant, J. T., Loubeau, A., Doebler, W. J., and Klos, J., "Reducing Contaminating Noise Effects When Calculating Low-Boom Loudness Levels," *The Journal of the Acoustical Society of America*, Vol. 155, No. 6, pp. 3889–3899, 2024. https://doi.org/10.1121/10.0026436

[30] Cliatt, L. J., Haering, E. A., Arnac, S. R., Hill, M. A., "Lateral Cutoff Analysis and Results from NASA's Farfield Investigation of No-Boom Thresholds," NASA/TM-2016-218850, 2016.

[31] Anderson, M. C., Doebler, W. J., Gee, K. L., Nyborg, K., Loubeau, A., "Comparing sonic boom turbulence-induced variability with computational models for the CarpetDIEM-I test campaign," The *Journal of the Acoustical Society of America,* Submitted 2025.

[32] Harker, B. M., Lympany, S. V., Page, J. A., "Performance Evaluation of a Shaped Sonic Boom Detector and Classifier," Presentation. 2022. https://ntrs.nasa.gov/citations/20220017378

[33] Doebler, W. J., Rathsam, J., "How loud is X-59's shaped sonic boom?" *Proceedings of Meetings on Acoustics,* 36 (1): 040005, 2019. https://doi.org/10.1121/2.0001265

[34] The MathWorks, Inc., "MATLAB R2024a" (2024).